Hole charge localization and band structures of p-doped GaN/InGaN and GaAs/InGaAs semiconductor heterostructures

2002 J. Phys.: Condens. Matter 14 5813

(http://iopscience.iop.org/0953-8984/14/23/312)

INSTITUTE OF PHYSICS PUBLISHING JOURNAL OF PHYSICS: CONDENSED MATTER

J. Phys.: Condens. Matter **14** (2002) 5813–5827 PII: S0953-8984(02)32769-3

Hole charge localization and band structures of p-doped GaN/InGaN and GaAs/InGaAs semiconductor heterostructures

S C P Rodrigues[1,3], G M Sipahi[2], L M R Scolfaro[1] and J R Leite[1]

[1] Instituto de Física, Universidade de São Paulo, CP 66318, 05315-970 São Paulo, SP, Brazil
[2] Instituto de Física de São Carlos, Universidade de São Paulo, CP 369, 13560-970 São Paulo, SP, Brazil

E-mail: sara@if.sc.usp.br (S C P Rodrigues) and scolfaro@if.usp.br

Received 16 January 2002, in final form 17 April 2002
Published 30 May 2002
Online at stacks.iop.org/JPhysCM/14/5813

Abstract

Hole band structures of p-doped semiconductor heterostructures are presented. The full six-band Luttinger–Kohn Hamiltonian generalized to treat different materials is solved in conjunction with the Poisson equation in a plane-wave representation. Self-consistent solutions of the multiband effective-mass–Poisson equations are obtained for unstrained and biaxially strained zinc-blende GaN/$In_xGa_{1-x}N$ and GaAs/$In_xGa_{1-x}As$ quantum wells and superlattices (SLs), in which the acceptor doping concentration and its profile, the SL period, and the alloy content x are varied. The particular features observed in the valence subband structure of GaN/InGaN systems are stressed in a comparison with other selected In-derived III–V heterostructures, such as GaAs/InGaAs SLs.

1. Introduction

In the past few years there has been a growing interest in the III–N-derived heterostructures, such as AlGaN/GaN and GaN/InGaN multiple quantum wells (QWs) and superlattices (SLs), due to their important applications in several devices [1,2]. The devices have been demonstrated in both the stable wurtzite (w) phase [1] and the cubic (c) [2] phase. Although most of the progress achieved so far is based on the wurtzite materials, the metastable c-phase layers are emerging as promising alternatives for similar applications [3, 4].

Controlled p-type doping of the III–N material layers is of crucial importance for electronic as well as for transport-based device performances. Nevertheless, this has proved to be difficult by virtue of the deep nature of the acceptors in the nitrides (around 0.1–0.2 eV above the top of the valence band in the bulk materials [5])—in contrast to the case for GaAs-derived

[3] Present address: Instituto de Física de São Carlos, Universidade de São Paulo, CP 369, 13560-970 São Paulo, SP, Brazil.

heterostructures, in which acceptor levels are only few millielectron volts apart from the band edge. Several attempts have been made to enhance the acceptor doping efficiency, for example by using multiple QWs and SLs made up of alternate layers of w-GaN and AlGaN or InGaN [6–8]. This also provided evidence for the formation of a two-dimensional hole gas (2DHG) in the well regions of the heterostructures, which is induced by piezoelectric (PZ) effects. Contrary to the case for wurtzite material systems, in p-doped cubic structures a 2DHG may arise, even in the absence of PZ fields.

For the description of the electronic structure of n-type doping in e.g. III–V heterostructures, the self-consistent solution of the one-band effective-mass equation (EME), in conjunction with the Poisson equation for the confined electron gas, suffices. In contrast, for p-doped systems the three uppermost heavy-hole, light-hole, and spin–orbit split-off-hole bands must be taken into consideration in a realistic calculation of the valence band structures and their related properties. The hole subbands of undoped w- and c-AlGaN/GaN multiple QWs and SLs have been calculated by several authors through the use of 6×6 Rashba–Sheka or Luttinger–Kohn (LK) Hamiltonians [9–12]. Similar calculations have also been reported for undoped arsenide-derived structures such as InGaAs/InP [13] and InGaAs/AlGaAs [14].

Self-consistent band-structure calculations for a hole gas in the most common III–V AlGaAs/GaAs QWs and SLs have been carried out by Kim and Majerfeld [15] and Kim *et al* [16] using the LK multiband EME of the Γ_8 and Γ_7 valence band complex. The anisotropy in the x–y plane (perpendicular to the growth axis z) has been neglected in these calculations. More complete self-consistent calculations were reported by Kemerink *et al* on p-doped asymmetric AlGaAs/GaAs double QWs [17] and p-type δ-doped multiple AlGaAs/GaAs QWs [18], which are based on the 4×4 LK model and include non-parabolicity in the x–y plane and exchange–correlation (XC) effects within the 2DHG. For doped nitride heterostructures, the investigations reported so far deal only with wurtzite systems such as magnesium-doped AlGaN/GaN single heterojunctions [19] or AlGaN/GaN QWs [20] and SLs [21]. From the published results we conclude that the self-consistent band-structure calculations carried out so far for a hole gas in the III–V QWs and SLs neglect important effects which, unlike in the AlGaAs/GaAs systems, are found to play important roles.

In previous works we have applied the $\boldsymbol{k} \cdot \boldsymbol{p}$ method within the framework of a plane-wave representation to calculate the hole band structures of undoped [12] and doped [22, 23] group-III nitride heterostructures. The aim of the present work is to report on self-consistent hole band-structure calculations, focusing on a detailed discussion of the hole charge localization in zinc-blende GaN/$In_xGa_{1-x}N$ and GaAs/$In_xGa_{1-x}As$ QWs and SLs. Preliminary results for selected p-type modulation doping in GaN/InGaN and AlGaN/GaN heterostructures have been reported by us [25]. Here a more detailed study is presented for GaN/InGaN along with a comparison with results for GaAs/InGaAs for which no self-consistent calculations have been reported so far. The multiband EME, which includes strain effects and the hetero-interface-derived potential is solved in conjunction with the Poisson equation for the carrier charge density. XC effects within the 2DHG are taken into account in a rigorous way, as was done in our previous investigations of p-type δ-doped layers [24]. Valence subband and miniband structures are obtained for the heterostructures in which the acceptor doping concentration and its profile, the SL period, i.e., well and barrier thicknesses, and the alloy content x are varied. The paper is organized as follows. In section 2 we describe the self-consistent 6×6 $\boldsymbol{k} \cdot \boldsymbol{p}$ method, with the generalized kinetic energy term in the multiband EME, adopted here to calculate the band structure for unstrained and biaxially strained layers, and show how the self-consistent potentials are obtained. In section 3 we present results for the GaN/InGaN and GaAs/InGaAs heterostructures studied. The role played by the use of different Luttinger parameters in these In-related systems is discussed. We emphasize the particular features of

the hole band structure in InGaN-derived QWs and SLs in contrast with those observed in the InGaAs systems. In section 4 we draw our conclusions.

2. Model and theoretical method

We adopt a model approach based on a supercell that comprises the QWs and barrier regions of a zinc-blende-based heterostructure. An infinite SL composed of a number n of square wells of thicknesses d_n, along the growth direction [001] coincident with the z axis, is assumed. The multiband EME is represented with respect to a basis set of plane waves, with wavevectors $K = (2\pi/d)l$ (l being an integer, and $d = d_1 + d_2 + \cdots + d_n$ the SL period) equal to the reciprocal-SL vectors [24]. The rows and columns of the 6×6 LK Hamiltonian refer to the Bloch-type eigenfunctions $|jm_j\boldsymbol{k})$ of the Γ_8 heavy- and light-hole bands, and the Γ_7 spin–orbit split-off-hole band; $\boldsymbol{k}$ denotes a vector of the first SL BZ. The expansion of the EME with respect to plane waves $(z|K)$ means representing this equation with respect to Bloch functions $(x|jm_j\boldsymbol{k} + Ke_z)$. For a Bloch-type eigenfunction $(z|\nu\boldsymbol{k})$ of the SL of energy E_ν, associated with the band index ν, and wavevector $\boldsymbol{k}$, the EME has the form

$$\sum_{j'm'_jK'} (jm_j\boldsymbol{k}K|H_0 + H_S + V_{HET} + V_A + V_H + V_{XC}|j'm'_j\boldsymbol{k}K')(j'm'_j\boldsymbol{k}K'|E_\nu\boldsymbol{k}) = E_\nu(\boldsymbol{k})(jm_j\boldsymbol{k}K|E_\nu\boldsymbol{k}), \tag{1}$$

where H_0 is the unperturbed kinetic energy term described by generalizing the $\boldsymbol{k}\cdot\boldsymbol{p}$ Hamiltonian for heterostructures. Details of this generalization are shown in the appendix. Here, the method is applied for $n = 2$. In equation (1), H_S is the strain term originating from the lattice mismatch between the different layers of the system, V_{HET} is the valence band discontinuity potential, V_A is the ionized acceptor charge distribution potential, V_H is the Hartree potential due to the hole charge distribution, and V_{XC} is the XC potential, considered within the local density approximation (further detailed expressions may be found in [22, 23, 25]). As the potentials V_H and V_{XC} entering equation (1) depend on the carrier charge distribution itself, one has to solve self-consistently the EME (equation (1)) and the Poisson equation for the Coulomb potential V_C, given by the sum of V_H and V_A, i.e.

$$(K|V_C|K') = \frac{4\pi e^2}{\varepsilon}\frac{1}{|K-K'|^2}[(K|N_A|K') - (K|p|K')], \tag{2}$$

where ε is the dielectric constant, and $(K|N_A|K')$ and $(K|p|K')$ are the Fourier coefficients of the ionized acceptor profile function $N_A(z)$ and of the hole charge distribution $p(z)$, respectively [23]. We assume in the calculations presented here a unique dielectric constant (ε) throughout the whole SL. We do not expect this assumption to lead to significant changes in subband energies and potential profiles. For the nitride-derived structures for which the hole effective masses are large, only a small amount of the charge density is found to penetrate the barriers. On the other hand, for the arsenide-based heterostructures the dielectric constants of wells and barriers differ only by a few per cent [26], or even less if we consider in particular small values of the alloy compositions as in the systems investigated here.

In order to take into account in the calculations the biaxial strain, we followed our previous work [22]. The biaxial strain can be decomposed into two terms: a hydrostatic term and an uniaxial term. Since the hydrostatic term changes the gap energy, thus not affecting the valence band potential depth, only the uniaxial strain component will be considered [27]. This latter may be calculated from the following expression:

$$\epsilon = -(2/3)D_u\epsilon_{xx}(1 + 2C_{12}/C_{11}), \tag{3}$$

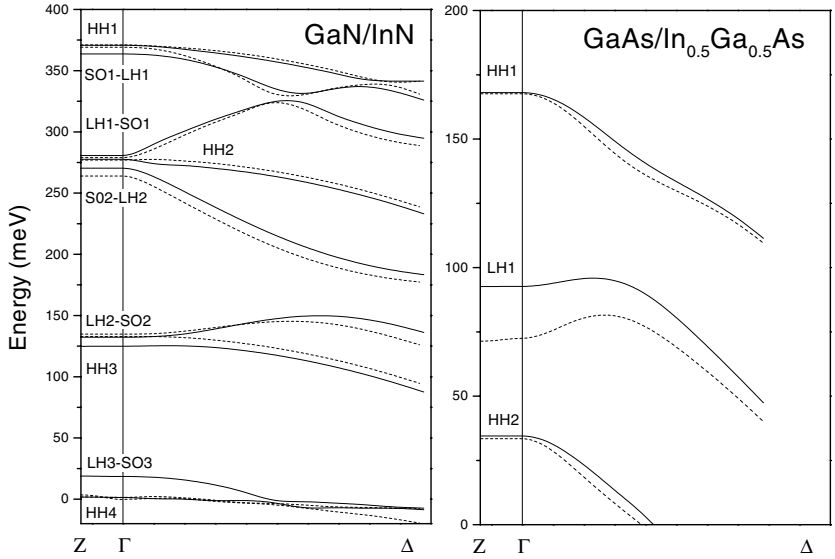

Figure 1. Valence band structures for undoped and unstrained multiple QWs along high-symmetry lines Γ–Z and Γ–Δ, with $d_1 = 200$ Å and $d_2 = 30$ Å. Left: GaN/InN; right: $GaAs/In_{0.5}Ga_{0.5}As$. Solid (dashed) curves correspond to different (equal) Luttinger parameters for barrier and well materials. The energy zero was taken at the top of the barrier. The labels LHi–SOi (SOi–LHi) refer to mixed light-hole and split-off-hole states with higher contributions of light holes (split-off holes) to the wavefunction at the Γ point.

where $-(2/3)D_u$ is the shear deformation potential, C_{11} and C_{12} are the elastic constants, and ϵ_{xx} is the lattice mismatch which is given by

$$\epsilon_{xx} = (a_{barrier} - a_{well})/a_{well}, \tag{4}$$

$a_{barrier}$ and a_{well} being the lattice parameters of the barrier and well materials, respectively.

3. Results and discussion

3.1. Undoped structures

We first discuss the influence of the use of different Luttinger parameters for the material layers forming the well and barrier regions in a heterostructure involving the systems investigated here. In figure 1 we depict band structures along the Γ–Z and Γ–Δ lines of the SL BZ for unstrained GaN/InN and $GaAs/In_{0.5}Ga_{0.5}As$ multiple QWs, with barrier thickness $d_1 = 200$ Å and well thickness $d_2 = 30$ Å. The Γ–Δ line corresponds to wavevectors k_x perpendicular to the SL axis (Γ–Z). The hole levels are labelled according to their main character at Γ. The notation SOi–LHi (LHi–SOi) means that the mixing character of band i is dominated by split-off holes (light holes). The parameters used in the calculations are displayed in table 1. The values of Δ, the spin–orbit splitting energy, the lattice parameter a, and the effective masses m^* for the binary GaN and InN compounds were obtained through *ab initio* fully relativistic linear augmented plane-wave (FLAPW) band-structure calculations [28] (except for the effective masses of InN, which were taken from [29]). For GaAs and InAs the values of these quantities, as well as all the other quantities needed for InN, have been extracted from the literature. The Luttinger parameters γ_i are connected to the effective masses by standard relations which may be found elsewhere [33]. For the alloys, the parameters were obtained

Table 1. Bulk parameters as obtained from *ab initio* calculations performed by us [28] and extracted from the literature. Effective masses are along the [001] direction in units of the free-electron mass.

	GaN	InN	GaAs	InAs
γ_1	2.83	3.77	7.65[a]	19.67[a]
γ_2	0.85	1.33	2.41[a]	8.37[a]
γ_3	1.14	1.60	3.28[a]	9.29[a]
Δ (meV)	14	3	0.34[a]	0.38[a]
a (Å)	4.55	5.03	5.65[a]	6.058[a]
m^*_{hh}	0.85	0.84[b]	0.34[c]	0.35[c]
m^*_{lh}	0.22	0.16[b]	0.094[c]	0.026[c]
m^*_{so}	0.34	0.24[b]	—	—
E_g^Γ (meV)	3.2	1.9[d]	1.52[c]	0.418[c]
$(2/3)D_u$ (eV)	1.6[e]	1.2[f]	2[a]	1.8[a]
C_{11} (GPa)	293[g]	187[g]	112.6[c]	83.3[c]
C_{12} (GPa)	159[g]	125[g]	57.1[c]	45.3[c]

[a] Reference [27].
[b] Reference [29].
[c] Reference [26].
[d] Reference [30].
[e] Reference [11].
[f] Reference [31].
[g] Reference [32].

by linearly interpolating between the bulk binary material values, except the energy gap of $In_xGa_{1-x}N$ for which we adopted a parabolic dependence on x, with a bowing parameter of 1.05 eV [30]. The values adopted for the dielectric constant were 9.5 [22] and 12.35 [26], for the nitride- and arsenide-based heterostructures, respectively, in units of the vacuum permittivity, ε_0. For the valence band offset we adopted 40% in both kinds of system [34].

As we can observe in figure 1, the effect of utilizing different effective-mass parameters is more pronounced for light-hole bands, due to their smaller effective masses. Similar behaviour was recently obtained by us for $Al_xGa_{1-x}N$/GaN multiple QWs [12]. These changes are found to increase with the alloy composition parameter x. In InGaAs-based structures, the effect of the use of different Luttinger parameters is particularly remarkable, since the light-hole mass in this case is even smaller. For the nitrides, by virtue of the coupling between light-hole and split-off-hole bands already being strong at the Γ point, the mixed SOi–LHi and LHi–SOi states are the ones which are more affected.

Another feature seen in figure 1 for the GaN/InN multiple QWs is that the HH and SO–LH states always show up in couples separated by $\approx\Delta$, the spin–orbit splitting energy. This may be explained by the very high values of the effective masses of the heavy holes and of the mixed split-off–light holes. As there is no dispersion along the Γ–Z direction for these large-period SLs, we only observe the folding of the subbands caused by the SL periodicity. This is no longer true in the case of the mixed light–split-off-hole bands, due to their much smaller effective mass.

3.2. Hole band structures and potentials of doped GaN/InGaN multiple QWs and SLs

In figure 2, schematic representations of the doping and potential profiles in a doped SL (or multiple QWs) are depicted. In order to allow a more rigorous analysis of the results, we will consider the 3D ionized acceptor concentration, N_A, as constant and fixed, and will increase the 2D acceptor concentration in our systems by increasing the thickness of the doping layer

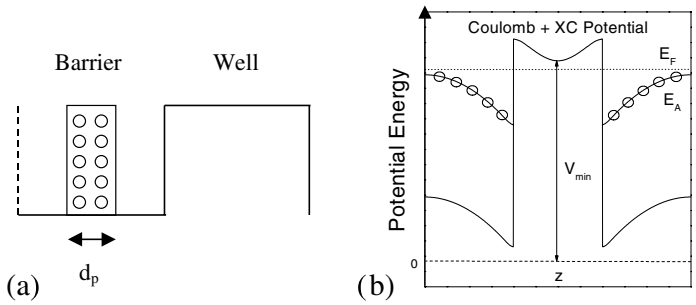

Figure 2. Schematic representations of doped multiple QWs: (a) the doping profile in the barrier, and (b) the corresponding potential profile. The Fermi level, E_F, the minimum of the potential depth, V_{min}, and the ionized acceptor level, E_A, are also indicated. The energy zero was placed at the Coulomb potential at the top of the barrier.

(d_p), which is placed at the centre of the barrier. This doping profile is shown schematically in figure 2(a). As the acceptor binding energies in group-III nitrides possess values between 0.1 and 0.2 eV [35], and in the systems investigated here the barrier heights are higher than 200 meV, we may safely assume in the calculations that all acceptors are ionized and the total hole density is equal to the total acceptor density.

The inclusion of XC effects in our calculations gives rise to different XC potentials for each different kind of hole [22]. In contrast, all particles feel the same total Coulomb potential. Therefore, an appropriate choice for a reference for the potential energy of the doped heterostructure would be the total Coulomb potential at the top of the barrier. Figure 2(b) shows this choice schematically. The energy zero has been placed at the top of the total Coulomb potential, and the potential depicted is the total potential, with the inclusion of the XC term. The ionized acceptor level (E_A), the Fermi level (E_F), and the minimum depth of the well due to the potential bending (V_{min}) are also represented. Because of the different XC energies, each kind of carrier will feel a different total potential.

In figure 3 we analyse the dependence of the hole subbands on the doping concentration. There we present the energy levels at the Γ point for strained GaN/$In_xGa_{1-x}N$ ($x = 0.3$) multiple QWs with $d_1 = 200$ Å and $d_2 = 100$ Å. For this alloy composition the barrier height is 240.4 meV and the wells are compressively strained ($\epsilon = 97.1$ meV). We assumed that all the parameters needed to calculate the strain could be linearly interpolated between the bulk values given in table 1. Since the critical thicknesses in the nitrides are still not well established, we were guided here by recent photoluminescence measurements carried out on wurtzite $In_xGa_{1-x}N$/GaN samples for x-values $\leqslant 0.2$ and by an analytical estimation [36] performed for cubic $Al_xGa_{1-x}N$ layers grown on GaN(001) for $0 \leqslant x \leqslant 1$ [37]. The 3D acceptor doping concentration is fixed at $N_A = 1 \times 10^{18}$ cm^{-3}, and the doping layer thickness, d_p, varies from 60 to 200 Å. According to the values of d_p, the 2D acceptor concentration varies in the interval 6×10^{11} cm$^{-2} < N_A^{2D} < 2 \times 10^{12}$ cm^{-2}. The Fermi level, E_F, and the minimum of the potential depth due to bending, V_{min}, are also shown. One can easily understand from the picture shown in figure 2 that the two lowest states (HH1 and HH2) appearing in figure 3 are a doublet, which results from the interaction of two different wells created by the bending of the potential caused by the self-consistent charge distribution. From here on, we will call these two interacting wells a double QW. This feature can indeed be inferred from the spatial localization of the wavefunctions associated with the HH1 and HH2 states (not shown), with the former symmetric and the latter asymmetric, both with maxima centred at each well

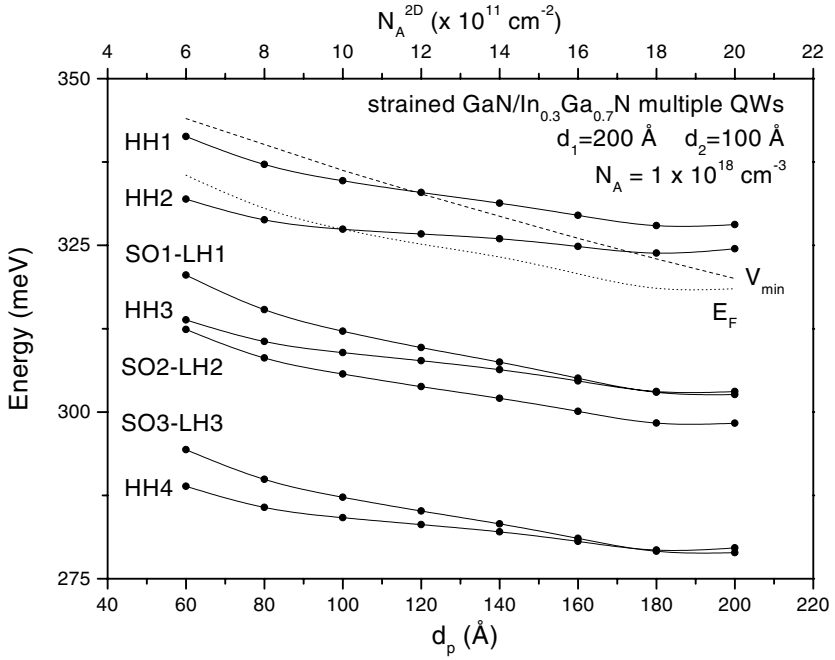

Figure 3. The lowest seven energy levels, the minimum of the potential depth, V_{min}, and the Fermi level, E_F, plotted against the doping layer thickness d_p (scale at the bottom), and against the 2D acceptor concentration N_A^{2D} (scale at the top) for strained GaN/$In_{0.3}Ga_{0.7}$N SLs with $d_1 = 200$ Å and $d_2 = 100$ Å. The energy zero and labels are as in figures 1 and 2.

forming the double QW. The crossings of the second heavy-hole subband (HH2) with E_F and with V_{min} allow us to divide the range of values of the doping layer thicknesses into three different regions: a region where only one subband is occupied ($d_p < 100$ Å), a region where two subbands are occupied and one can see a transition from a single QW to a double QW (100 Å $< d_p <$ 170 Å), and a region where two subbands are occupied in a double QW ($d_p > 170$ Å). These findings may have important implications in the interpretation of optical measurements, e.g. photoluminescence spectra, for nitride-based heterostructures.

From figure 3 one can also note that the minimum of the potential depth (V_{min}) decreases almost linearly with the increase of N_A^{2D}. This behaviour is expected since the potential bending is enhanced by the increase of N_A^{2D}. A different behaviour (not linear) is observed for the trend in the position of the energy levels. This difference can be explained on the basis of the different regions defined above. In the singly occupied subband region, the increase of the bending pushes down the levels towards the top of the barrier, delocalizing them. In the transition region this effect is less pronounced due to the fact that two distinct subbands are being occupied. In the double QW region, the increase of the hole density enhances the localization of the holes, pulling the levels up towards the bottom of the well.

In order to emphasize the degree of localization of the hole charge density distribution in such systems, we show in figure 4 a contour plot of the 3D hole density as a function of z, $p(z)$, for the same systems as were shown in figure 3. As in figure 3, d_p varies from 60 to 200 Å. One can see from this figure that for smaller 2D hole concentrations, $p(z)$ has a maximum at the centre of the well, with a broad distribution. As the 2D hole concentration increases, the system starts to present two maxima. The charge distribution profile shown in

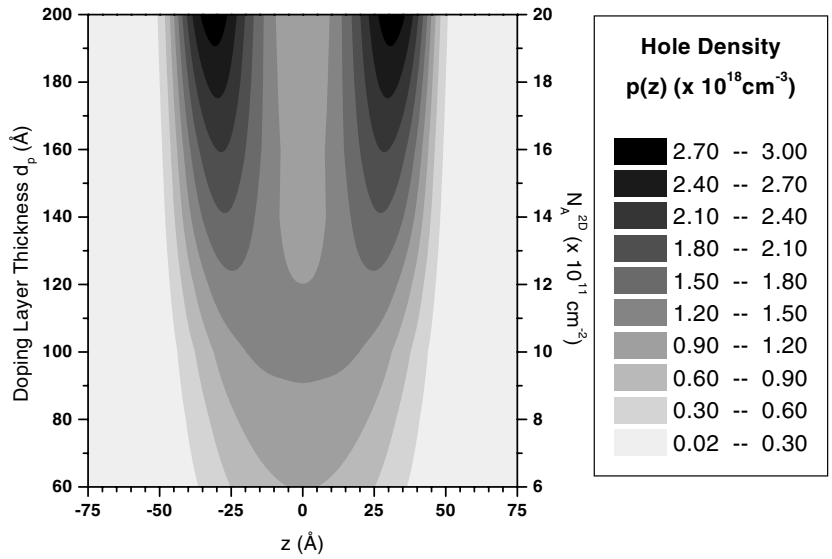

Figure 4. A contour plot showing the hole density distribution $p(z)$ along the growth axis z for a strained GaN/$In_{0.3}Ga_{0.7}N$ multiple QW, with $d_1 = 200$ Å and $d_2 = 100$ Å. The doping layer thickness d_p is varied from 60 to 200 Å (scale on the left), and the corresponding 2D acceptor concentration N_A^{2D} varied from 6 to 20 $\times$ 10^{11} cm^{-2} (scale on the right).

figure 4 indicates a behaviour similar to the one seen in figure 3, where the majority of the charge density is concentrated inside the double QW defined by the potential bending and the QW barriers. Therefore, for higher N_A^{2D} (above 1.2×10^{12} cm^{-2}), one can assume that two different carrier channels are present in these systems.

3.3. Doped GaAs/InGaAs systems: isolated wells and SLs

This section is devoted to the presentation of results for doped GaAs/InGaAs heterostructures, and to a comparison of the results with those for GaN/InGaN systems. We have chosen heterostructures which involve InGaAs layers, since biaxial strain also plays a role if these layers are on top of GaAs for example. In figure 5 we show the valence band structure, potential profiles, and Fermi level position for an unstrained GaAs/$In_xGa_{1-x}As$ ($x = 0.3$) SL, with $d_1 = 40$ Å, $d_2 = 30$ Å, in which the GaAs barriers are fully doped. The 2D doping concentration is $N_A^{2D} = 6 \times 10^{12}$ cm^{-2} ($N_A = 1.5 \times 10^{19}$ cm^{-3}) and the valence band barrier height is 132.2 meV. For such small period the strain in the SL may be considered as compensated [38], i.e., one can assume in the calculation an unstrained system. Since the spin–orbit splitting energy is large in this case (see table 1), the influence of the split-off band is negligible, as expected. One can observe a remarkable SL behaviour, which is apparent from the miniband dispersions along the Γ–Z direction. Even the first heavy-hole level (HH1) shows a noticeable dispersion. Two minibands are found to be occupied for this short-period SL. Two main characteristics are responsible for the particular features of the system: the barrier heights and the values of the effective masses. Since the hole effective masses for the arsenides are in general much smaller than those for the nitrides, the valence states in the former are expected to be more delocalized. This delocalization is still enhanced by the shallower nature of the barrier height. It is interesting to note that, contrarily to what has been observed for the nitride-based QWs and SLs, the Fermi level now approaches the top of the

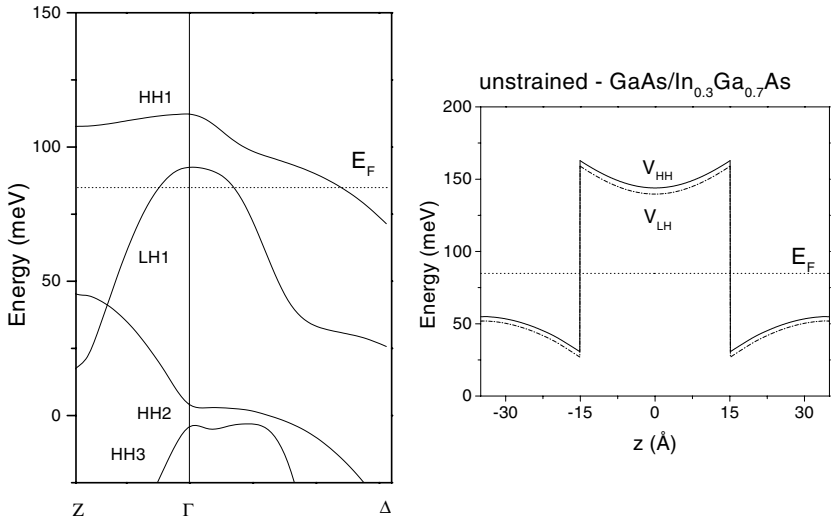

Figure 5. Valence band structure (left) and potential profiles (right) for an unstrained fully doped barrier GaAs/$In_{0.3}Ga_{0.7}As$ SL, with $d_1 = 40$ Å and $d_2 = 30$ Å, and $N_A = 1.5 \times 10^{19}$ cm^{-3} ($N_A^{2D} = 6 \times 10^{12}$ cm^{-2}). E_F indicates the Fermi level. The energy zero and labels are as in figure 3.

barrier, and the first light-hole miniband (LH1) is also found occupied. Besides, contrary to the case for GaN/InGaN, in the GaAs/InGaAs-based structures, with the same well and barrier thicknesses, very broad minibands occur, characterizing very strong interacting wells. Since the acceptor level binding energy in GaAs if of ≈26–30 meV (usually C or Be) [26], 2D hole gases of at least 50% higher densities can be achieved.

In figure 6 the hole band structure, potential profiles, and Fermi level position are depicted for a compressively strained GaAs/$In_xGa_{1-x}As$ multiple QW ($x = 0.3$) with a larger period, $d_1 = 200$ Å and $d_2 = 100$ Å, and fully doped barriers with $N_A^{2D} = 2 \times 10^{12}$ cm^{-2} ($N_A = 1 \times 10^{18}$ cm^{-3}). The value of the strain energy is $\varepsilon = 83.5$ meV. For this system the effective heavy-hole potential well, V_{HH}, becomes more than four times deeper than the light-hole potential well, V_{LH} (see the right-hand side of figure 6). As a consequence, the first seven minibands are of heavy-hole character at Γ. Even if we consider the parallel Γ–Δ direction, where a mixing of heavy- and light-hole states takes place, and therefore the well known strong anti-crossing behaviour is expected [24], one can still see the effects of the strong heavy-hole character which is revealed by the small non-parabolicity of the (parallel) subbands. Examining the mixed light–split-off-hole (LHi–SOi) bands, one observes a very small degree of split-off-hole character; this is explained by the fact that the split-off-hole potential well lies inside the continuum energy region defined by the others—the heavy- and light-hole potentials. It is worth mentioning that, nevertheless, the split-off band should be included in the self-consistent calculation since it does influence the valence band structure, particularly that of strained systems.

We may also compare the results depicted in figure 6 with that shown in figure 4 for GaN/InGaN, considering in the latter the same values of d_p and N_A^{2D} as were used for GaAs/InGaAs. The two different carrier channels seen for GaN/InGaN, and characterized by the localization of the hole charge density within the double QW, are not observed for the GaAs/InGaAs system.

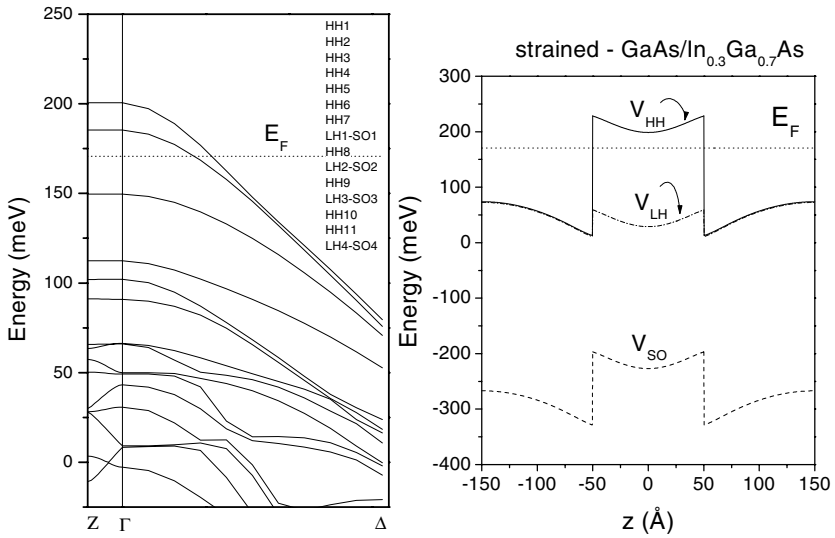

Figure 6. Valence band structure (left) and potential profiles (right) for a strained fully doped barrier GaAs/$In_{0.3}Ga_{0.7}As$ SL, with $d_1 = 200$ Å and $d_2 = 100$ Å, and $N_A = 1 \times 10^{18}$ cm^{-3}. E_F indicates the Fermi level. The energy zero and labels are as in figure 3. The split-off-hole potential, V_{SO}, has been shifted by Δ relative to the heavy-hole potential, V_{HH}.

4. Conclusions

We have presented a self-consistent $\boldsymbol{k} \cdot \boldsymbol{p}$ method generalized to investigate p-type doped heterostructures with any valence band potential profile, which includes biaxial strain and XC effects in the 2DHG within the local density approximation. The method relies on a plane-wave expansion of the full six-band LK Hamiltonian which is solved together with the Poisson equation, in the reciprocal space. The method is applied to study the valence subband and miniband structures, potential profiles, and Fermi level positions in In-based heterostructures. Results were presented for zinc-blende GaN/InGaN and GaAs/InGaAs multiple QWs and SLs, in which the acceptor doping concentration, the superlattice period, and the alloy composition were varied. The use of different Luttinger parameters, associated with the distinct materials comprising the heterostructure, affects particularly the light-hole bands due to their smaller effective masses. It is demonstrated that in the case of InGaAs-derived structures this effect can be very drastic, especially for higher In content.

For p-doped GaN/$In_xGa_{1-x}N$ SLs and multiple QWs, only if $x \geqslant 0.3$ is the existence of a confined 2DHG likely, by virtue of the deep nature of the acceptor levels ($\sim$200 meV) in the nitrides. For $x \sim 0.3$ and multiple QWs with barriers 200 Å wide, the highest acceptor concentration which can be achieved is of the order of 1×10^{18} cm^{-3}, corresponding to 2DHG densities of about 2×10^{12} cm^{-2}. Minibands with significant dispersion are found to occur only for periods $\leqslant$100 Å and mostly for higher light–split-off mixed bands. The remarkable differences seen in the GaAs/InGaAs structures when compared to GaN/InGaN were emphasized. In particular for the latter, the presence of a p-doping-induced double carrier channel is found, due to the large values of effective masses in the nitrides. This is an interesting feature for device application.

No attempts were made by us here to make direct comparisons between our calculations and experimental results. Although there exists a vast literature on e.g. luminescence of nitride-based heterostructures, studies have mostly been performed on wurtzite materials. For the cubic

phase of the nitrides, only more recently have GaN/InGaN/GaN double heterostructures grown on GaAs(001) substrates [39–41] and InGaN/GaN QW structures grown on 3C–SiC(001) substrates [42–44] been reported. The origin of the electronic transitions seen in InGaN/GaN heterostructures is still a subject of discussion. There is strong evidence that these transitions arise from phase-separated quantum dots in the relaxed InGaN layers. However, in strained films the phase separation may be suppressed [45]. In this case, therefore, the QW electronic transitions can be observed [46]. Studies of the optical properties of QWs and SLs based on cubic nitrides will certainly provide important guidelines for the interpretation of forthcoming experiments.

Acknowledgments

We thank FAPESP and CNPq (Brazilian funding agencies) for partial support of this work. One of us (SCPR) thanks Professor G H Döhler for many fruitful discussions and for a critical reading of the manuscript.

Appendix

We start by considering the SL of period d with a primitive unit cell consisting of n different material layers. An effective-mass parameter $f(z)$, which assumes a certain value for each different region of the system, can be expressed by the general form

$$f(z) = \begin{cases} f_1 & d_0 \leqslant z \leqslant d_1 \\ f_2 & d_1 \leqslant z \leqslant d_2 \\ f_3 & d_2 \leqslant z \leqslant d_3 \\ \vdots & \\ f_n & d_{n-1} \leqslant z \leqslant d_n \end{cases} \qquad \text{where} \begin{cases} d_0 = -\dfrac{d}{2} \\ d_n = \dfrac{d}{2}. \end{cases} \tag{A.1}$$

In order to describe the kinetic energy term of the unperturbed Hamiltonian, we need the momentum operator $\hat{p} = -\mathrm{i}\hbar\nabla$ expressed in terms of plane-wave functions $\mathrm{e}^{-\mathrm{i}Kz}$, i.e.

$$\hat{p} = -\mathrm{i}\hbar\nabla \Rightarrow \begin{cases} \hat{p}_x = -\mathrm{i}\hbar\dfrac{\partial}{\partial x} \\ \hat{p}_y = -\mathrm{i}\hbar\dfrac{\partial}{\partial y} \\ \hat{p}_z = -\mathrm{i}\hbar\dfrac{\partial}{\partial z}. \end{cases} \tag{A.2}$$

As both operators, the Luttinger parameters, and the momentum vary along the growth direction, it is necessary to determine their commutation relations and symmetrize the operators in their final form. So, for the general parameter $f(z)$, one has

$$\begin{aligned} &f(z) \Rightarrow f(z) \\ &f(z)\hat{p}_z \Rightarrow \tfrac{1}{2}[f(z)\hat{p}_z + \hat{p}_z^{\dagger} f(z)] \\ &f(z)\hat{p}_z\hat{p}_z \Rightarrow \hat{p}_z^{\dagger} f(z)\hat{p}_z. \end{aligned} \tag{A.3}$$

Applying these operators to the matrix elements of H_0 in equation (1), one has

$$\langle K|f(z)|K'\rangle = \frac{1}{d}\left[\int_0^d \mathrm{e}^{-\mathrm{i}Kz} f(z)\mathrm{e}^{\mathrm{i}K'z}\,\mathrm{d}z\right], \tag{A.4}$$

$$\langle K|\frac{1}{2}[p_z^\dagger f(z) + f(z)p_z]|K'\rangle = \frac{1}{d}\left\{\int_0^d \mathrm{e}^{-\mathrm{i}Kz}\frac{1}{2}[p_z^\dagger f(z) + f(z)p_z]\mathrm{e}^{\mathrm{i}K'z}\,\mathrm{d}z\right\}$$
$$= \frac{\hbar(K'+K)}{2d}\int_0^d \mathrm{e}^{-\mathrm{i}Kz} f(z)\mathrm{e}^{\mathrm{i}K'z}\,\mathrm{d}z, \tag{A.5}$$

and

$$\langle K|p_z^\dagger f(z)p_z|K'\rangle = \frac{1}{d}\int_0^d \mathrm{e}^{-\mathrm{i}Kz} p_z^\dagger f(z)p_z\mathrm{e}^{\mathrm{i}K'z}\,\mathrm{d}z = \frac{\hbar^2}{d}KK'\int_0^d \mathrm{e}^{-\mathrm{i}Kz} f(z)\mathrm{e}^{\mathrm{i}K'z}\,\mathrm{d}z. \tag{A.6}$$

Examining these integrals, one can find two distinct cases: when both sides of the matrix element have the same K and when the sides have different Ks.

As all three of the expressions (A.4)–(A.6) depend on the value of the integral $\int_0^d f(z)\mathrm{e}^{\mathrm{i}(K-K)z}\,\mathrm{d}z$, one has to determine the value of this integral in the two different cases. For $K' = K$, one has a very simple sum given by

$$\int_0^d f(z)\mathrm{e}^{\mathrm{i}(K-K)z}\,\mathrm{d}z = \sum_{i=1}^n f_i(d_i - d_{i-1}). \tag{A.7}$$

For $K' \neq K$, the integral is given by

$$\int_0^d f(z)\mathrm{e}^{\mathrm{i}(K'-K)z}\,\mathrm{d}z = -\mathrm{i}\frac{1}{(K'-K)}\left[(f_n - f_1) + \sum_{i=1}^{n-1}(f_i - f_{i+1})\mathrm{e}^{\mathrm{i}(K'-K)d_i}\right]. \tag{A.8}$$

Applying the above expressions (A.7) and (A.8) to the three different cases in (A.4)–(A.6), we have for $K' = K$

$$\langle K|f(z)|K\rangle = \frac{1}{d}\sum_{i=1}^n f_i(d_i - d_{i-1}) \tag{A.9}$$

$$\langle K|\tfrac{1}{2}[p_z f(z) + f(z)p_z]|K\rangle = \frac{\hbar K}{d}\sum_{i=1}^n f_i(d_i - d_{i-1}) \tag{A.10}$$

$$\langle K|p_z f(z)p_z|K\rangle = \frac{\hbar^2K^2}{d}\sum_{i=1}^n f_i(d_i - d_{i-1}) \tag{A.11}$$

and for $K' \neq K$

$$\langle K|f(z)|K'\rangle = -\mathrm{i}\frac{1}{d}\frac{1}{(K'-K)}\left[(f_n - f_1) + \sum_{i=1}^{n-1}(f_i - f_{i+1})\mathrm{e}^{\mathrm{i}(K'-K)d_i}\right] \tag{A.12}$$

$$\langle K|\tfrac{1}{2}[p_z^\dagger f(z) + f(z)p_z]|K'\rangle = -\mathrm{i}\frac{\hbar}{2d}\frac{(K+K')}{(K'-K)}\left[(f_n - f_1) + \sum_{i=1}^{n-1}(f_i - f_{i+1})\mathrm{e}^{\mathrm{i}(K'-K)z_i}\right] \tag{A.13}$$

$$\langle K|p_z f(z)p_z|K'\rangle = -\mathrm{i}\frac{\hbar^2}{d}\frac{KK'}{(K'-K)}\left[(f_n - f_1) + \sum_{i=1}^{n-1}(f_i - f_{i+1})\mathrm{e}^{\mathrm{i}(K'-K)d_i}\right]. \tag{A.14}$$

Replacing the operators in the kinetic energy matrix (H_0) of equation (1), we obtain $(jm_j\boldsymbol{k}K|T|j'm_j'\boldsymbol{k}K')$

$$= \begin{pmatrix} \hat{Q} & \hat{S} & \hat{R} & 0 & \frac{\mathrm{i}}{\sqrt{2}}\hat{S} & -\mathrm{i}\sqrt{2}\hat{R} \\ \hat{S}^* & \hat{T} & 0 & \hat{R} & \frac{-\mathrm{i}}{\sqrt{2}}(\hat{Q}-\hat{T}) & \mathrm{i}\sqrt{\frac{3}{2}}\hat{S} \\ \hat{R}^* & 0 & \hat{T} & -\hat{S} & -\mathrm{i}\sqrt{\frac{3}{2}}\hat{S}^* & \frac{-\mathrm{i}}{\sqrt{2}}(\hat{Q}-\hat{T}) \\ 0 & \hat{R}^* & -\hat{S}^* & \hat{Q} & -\mathrm{i}\sqrt{2}\hat{R}^* & \frac{-\mathrm{i}}{\sqrt{2}}\hat{S}^* \\ \frac{-\mathrm{i}}{\sqrt{2}}\hat{S}^* & \frac{\mathrm{i}}{\sqrt{2}}(\hat{Q}-\hat{T}) & \mathrm{i}\sqrt{\frac{3}{2}}\hat{S} & \mathrm{i}\sqrt{2}\hat{R} & \frac{1}{2}(\hat{Q}+\hat{T})-\hat{\Delta} & 0 \\ \mathrm{i}\sqrt{2}\hat{R}^* & -\mathrm{i}\sqrt{\frac{3}{2}}\hat{S}^* & \frac{\mathrm{i}}{\sqrt{2}}(\hat{Q}-\hat{T}) & \frac{\mathrm{i}}{\sqrt{2}}\hat{S} & 0 & \frac{1}{2}(\hat{Q}+\hat{T})-\hat{\Delta} \end{pmatrix}, \tag{A.15}$$

where $\hat{Q}$, $\hat{T}$, $\hat{S}$, and $\hat{R}$ are given by

$$\hat{Q} = -\frac{\hbar^2}{2m_0}\frac{1}{d}\left[\left(\sum_1^n(\gamma_1^i+\gamma_2^i)(d_i-d_{i-1})\right)(k_x^2+k_y^2) + K^2\sum_1^n(\gamma_1^i-2\gamma_2^i)(d_i-d_{i-1})\right] \tag{A.16}$$

$$\hat{T} = -\frac{\hbar^2}{2m_0}\frac{1}{d}\left[\left(\sum_1^n(\gamma_1^i-\gamma_2^i)(d_i-d_{i-1})\right)(k_x^2+k_y^2) + K^2\sum_1^n(\gamma_1^i+2\gamma_2^i)(d_i-d_{i-1})\right] \tag{A.17}$$

$$\hat{S} = \mathrm{i}\frac{\hbar^2}{2m_0}\frac{2\sqrt{3}}{d}(k_x-\mathrm{i}k_y)K\sum_1^n\gamma_3^i(d_i-d_{i-1}) \tag{A.18}$$

$$\hat{R} = -\frac{\hbar^2}{2m_0}\frac{\sqrt{3}}{d}\left[\left(\sum_1^n\gamma_2^i(d_i-d_{i-1})\right)(k_x^2-k_y^2) - 2\mathrm{i}\left(\sum_1^n\gamma_3^i(d_i-d_{i-1})\right)k_xk_y\right] \tag{A.19}$$

$$\hat{\Delta} = \frac{1}{d}\sum_1^n\Delta_i(d_i-d_{i-1}) \tag{A.20}$$

for $K' = K$, and by

$$\begin{aligned}\hat{Q} = \frac{\mathrm{i}\hbar^2}{2m_0}\frac{1}{(K'-K)}\frac{1}{d}\Bigg\{&\left[(\gamma_1^n+\gamma_2^n)-(\gamma_1^1+\gamma_2^1)+\sum_{i=1}^{n-1}[(\gamma_1^i+\gamma_2^i)-(\gamma_1^{i+1}+\gamma_2^{i+1})]\mathrm{e}^{\mathrm{i}(K'-K)z_i}\right]\\ &\times(k_x^2+k_y^2)+\Bigg[(\gamma_1^n-2\gamma_2^n)-(\gamma_1^1-2\gamma_2^1)\\ &+\sum_{i=1}^{n-1}[(\gamma_1^i-2\gamma_2^i)-(\gamma_1^{i+1}-2\gamma_2^{i+1})]\mathrm{e}^{\mathrm{i}(K'-K)z_i}\Bigg]KK'\Bigg\}\end{aligned} \tag{A.21}$$

$$\begin{aligned}\hat{T} = \frac{\mathrm{i}\hbar^2}{2m_0}\frac{1}{(K'-K)}\frac{1}{d}\Bigg\{&\left[(\gamma_1^n-\gamma_2^n)-(\gamma_1^1-\gamma_2^1)+\sum_{i=1}^{n-1}[(\gamma_1^i-\gamma_2^i)-(\gamma_1^{i+1}-\gamma_2^{i+1})]\mathrm{e}^{\mathrm{i}(K'-K)z_i}\right]\\ &\times(k_x^2+k_y^2)+\Bigg[(\gamma_1^n+2\gamma_2^n)-(\gamma_1^1+2\gamma_2^1)\\ &+\sum_{i=1}^{n-1}[(\gamma_1^i+2\gamma_2^i)-(\gamma_1^{i+1}+2\gamma_2^{i+1})]\mathrm{e}^{\mathrm{i}(K'-K)z_i}\Bigg]KK'\Bigg\}\end{aligned} \tag{A.22}$$

$$\hat{S} = \frac{\hbar^2}{2m_0}\frac{2\sqrt{3}}{d}(k_x-\mathrm{i}k_y)\frac{(K'+K)}{(K'-K)}\left[(\gamma_3^n-\gamma_3^1)+\sum_{i=1}^{n-1}(\gamma_3^i-\gamma_3^{i+1})\mathrm{e}^{\mathrm{i}(K'-K)d_i}\right] \tag{A.23}$$

$$\hat{R} = \mathrm{i}\frac{\hbar^2}{2m_0}\frac{1}{(K'-K)}\frac{\sqrt{3}}{d}\left\{\left[(\gamma_2^n-\gamma_2^1)+\sum_{i=1}^{n-1}(\gamma_2^i-\gamma_2^{i+1})\mathrm{e}^{\mathrm{i}(K'-K)d_i}\right](k_x^2-k_y^2)\right.$$
$$\left.-\mathrm{i}\left[(\gamma_3^n-\gamma_3^1)+\sum_{i=1}^{n-1}(\gamma_3^i-\gamma_3^{i+1})\mathrm{e}^{\mathrm{i}(K'-K)d_i}\right]k_xk_y\right\} \tag{A.24}$$

$$\hat{\Delta} = -\mathrm{i}\frac{1}{d}\frac{1}{(K'-K)}\left[(\Delta_n-\Delta_1)+\sum_{i=1}^{n-1}(\Delta_i-\Delta_{i+1})\mathrm{e}^{\mathrm{i}(K'-K)d_i}\right] \tag{A.25}$$

for $K' \neq K$.

References

[1] See, e.g.,
Nakamura S 1999 *Semicond. Sci. Technol.* **14** R27
Nakamura S and Fasol G 1997 *The Blue Laser Diode* (Berlin: Springer)
[2] Orton J W and Foxon C T 1998 *Rep. Prog. Phys.* **61** 1
[3] As D J, Richter A, Busch J, Lübbers M, Mimkes J and Lischka K 2000 *Appl. Phys. Lett.* **76** 13
[4] Holst J, Hoffmann A, Broser I, Schöttker B, As D J, Schikora D and Lischka K 1999 *Appl. Phys. Lett.* **74** 1966
[5] Pankove J I and Moustakas T D (ed) 1998 *Gallium Nitride (GaN): I (Semiconductors and Semimetals vol 50)* (San Diego, CA: Academic)
[6] Saxler A, Mitchel W C, Kung P and Razeghi M 1999 *Appl. Phys. Lett.* **74** 2023
[7] Kozodoy P, Hansen M, DenBaars S P and Mishra U K 1999 *Appl. Phys. Lett.* **74** 3681
[8] Kumakura K, Makimoto T and Kobayashi N 2000 *Japan. J. Appl. Phys.* **39** L195
Kumakura K, Makimoto T and Kobayashi N 2000 *Japan. J. Appl. Phys.* **39** 2428
[9] Sirenko Yu M, Jeon J-B, Kim K W, Littlejohn M A and Stroscio M A 1996 *Appl. Phys. Lett.* **69** 2504
Sirenko Yu M, Jeon J B, Lee B C, Kim K W, Littlejohn M A, Stroscio M A and Iafrate G J 1997 *Phys. Rev.* B **55** 4360
[10] Suzuki M and Uenoyama T 1996 *J. Appl. Phys.* **80** 6868
[11] Fan W J, Li M F, Chong T C and Xia J B 1996 *J. Appl. Phys.* **80** 3471
[12] Rodrigues S C P, Scolfaro L M R, Leite J R and Sipahi G M 2000 *Appl. Phys. Lett.* **76** 1015
[13] Ahn D, Yoon S J, Chuang S L and Chang C-S 1995 *J. Appl. Phys.* **78** 2489
[14] Lee J, Shieh C and Vassel M O 1991 *J. Appl. Phys.* **69** 1882
[15] Kim B W and Majerfeld A 1995 *J. Appl. Phys.* **77** 4552
[16] Kim B W, Mao E and Majerfeld A 1997 *J. Appl. Phys.* **81** 1883
[17] Kemerink M, Koenraad P M, Christianen P C M, Geim A K, Maan J C, Wolter J H and Henini M 1996 *Phys. Rev.* B **53** 10 000
[18] Kemerink M, Thomassen P M M, Koenraad P M, Bobbert P A, Henning J C M and Wolter J H 1998 *Phys. Rev.* B **58** 1424
[19] Hsu L and Walukiewicz W 1999 *Appl. Phys. Lett.* **74** 2405
[20] Park S-H and Chuang S-L 1998 *Appl. Phys. Lett.* **72** 3103
[21] Goepfert I D, Schubert E F, Osinsky A, Norris P E and Faleev N N 2000 *J. Appl. Phys.* **88** 2030
[22] Rodrigues S C P, Sipahi G M, Scolfaro L M R and Leite J R 2001 *J. Phys.: Condens. Matter* **13** 3381
[23] Rodrigues S C P, Sipahi G M, Scolfaro L M R and Leite J R 2001 *Physica* B **302–3** 106
[24] Rosa A L, Scolfaro L M R, Enderlein R, Sipahi G M and Leite J R 1998 *Phys. Rev.* B **58** 15 675
[25] Rodrigues S C P, Scolfaro L M R, Leite J R and Sipahi G M 2000 *Proc. Int. Workshop on Nitride Semiconductors (IPAP Conf. Ser. vol 1)* p 74
[26] Harbeke G, Madelung O and Rössler U 1982 *Landolt–Börnstein New Series* Group III, vol 17, ed O Madelung (Berlin: Springer)
[27] Pearsal T P 1990 *Strained-Layer Superlattices: Physics (Semiconductors and Semimetals vol 32)* (San Diego, CA: Academic)
[28] Ramos L E, Teles L K, Scolfaro L M R, Castineira J L P, Rosa A L and Leite J R 2001 *Phys. Rev.* B **63** 165210
[29] Pugh S K, Dugdale D J, Brand S and Abram R A 1999 *Semicond. Sci. Technol.* **14** 23
[30] Lemos V, Silveira E, Leite J R, Tabata A, Trentin R, Scolfaro L M R, Frey T, As D J, Schikora D and Lischka K 2000 *Phys. Rev. Lett.* **84** 3666
[31] Tadjer A, Abbar B, Rezki M, Aourag H and Certier M 1999 *J. Phys. Chem. Solids* **60** 419
[32] Wright A F 1997 *J. Appl. Phys.* **82** 2833
[33] Enderlein R, Sipahi G M, Scolfaro L M R and Leite J R 1998 *Phys. Status Solidi* b **206** 623

[34] The valence band offset in nitride-based hetero-interfaces has been discussed by several authors. See, e.g.,
Manz Ch, Kunzer M, Obloh H, Ramakrishnan A and Kaufmann U 1999 *Appl. Phys. Lett.* **74** 3993
Wei S-H and Zunger A 1996 *Appl. Phys. Lett.* **69** 2719
Martin G *et al* 1996 *Appl. Phys. Lett.* **68** 2541

[35] Marques M, Ramos L E, Scolfaro L M R, Teles L K and Leite J R 2001 *Proc. 25th Int. Conf. on Physics of Semiconductors (Osaka, Japan)* ed N Miura and T Ando, p 1411

[36] Parker C A, Roberts J C, Bedair S M, Reed M J, Liu S X and El-Masry N A 1999 *Appl. Phys. Lett.* **75** 2776
Reed M J, El-Masry N A, Parker C A, Roberts J C and Bedair S M 2000 *Appl. Phys. Lett.* **77** 4121

[37] Frey T, As D J, Bartels M, Pawlis A, Lischka K, Tabata A, Fernandez J R L, Silva M T O, Leite J R, Haug C and Brenn R 2001 *J. Appl. Phys.* **89** 2631

[38] Sęk G, Misiewicz J, Radziewicz D, Tłaczała M, Panek M and Korbutowicz R 1998 *Vacuum* **50** 219

[39] Tabata A, Teles L K, Frey T, Kharchenko A, Furthmüller J, Scolfaro L M R, As D J, Schikora D, Lischka K, Bechstedt F and Leite J R 2001 *Proc. 25th Int. Conf. on Physics of Semiconductors (Osaka, Japan)* ed N Miura and T Ando, p 1537

[40] Husberg O, Khartchenko A, As D J, Vogelsang H, Frey T, Schikora D, Lischka K, Noriega O C, Tabata A and Leite J R 2001 *Appl. Phys. Lett.* **79** 1243

[41] Taniyasu Y, Suzuki K, Lim D H, Jia A W, Shimotomai M, Kato Y, Kobayashi M, Yoshikawa A and Takahashi K 2000 *Phys. Status Solidi* a **180** 241

[42] Kitamura T, Cho S-H, Ishida Y, Ide T, Shen X-Q, Nakanishi H, Chichibu S F and Okumura H 2001 *J. Cryst. Growth* **227–8** 471

[43] Kitamura T, Suzuki Y, Ishida Y, Shen X-Q, Nakanishi H, Chichibu S F, Shimizu M and Okumura H 2001 *Phys. Status Solidi* a **188** 705

[44] Chichibu S F, Sugiyama M, Onuma T, Kitamura T, Nakanishi H, Kuroda T, Takeuchi A, Sota T, Ishida Y and Okumura H 2001 *Appl. Phys. Lett.* **79** 4319

[45] Tabata A, Teles L K, Scolfaro L M R, Leite J R, Kharchenko A, Frey T, As D J, Schikora D, Lischka K, Furthmüller J and Bechstedt F 2002 *Appl. Phys. Lett.* **80** 769

[46] Rodrigues S C P, Sipahi G M, Enderlein R, Scolfaro L M R, Noriega O C, Leite J R, Frey T, As D J, Schikora D and Lischka K 2002 *Phys. Status Solidi* a **190** 121